The Production of NO_2 from the Photolysis of Peroxyacetyl Nitrate

Troy L. Mazely*, Randall R. Friedl, and Stanley P. Sander#
Jet Propulsion Laboratory
California Institute of Technology
4800 Oak Grove Dr.
Pasadena, California 91109

*Present Address: Department of Earth System Sciences, University of California, Irvine, CA 92717
#To whom correspondence should be addressed.

Abstract

Peroxyacetyl nitrate (PAN) vapor was photolyzed at 248 nm and the NO_2 photoproduct was detected by laser induced fluorescence. The quantum yield for the production of NO_2 from PAN photolysis was determined by comparison to HNO_3 photolysis data taken under identical experimental conditions. The average of data collected over a range of total pressures, precursor concentrations, and buffer gases was 0.83 ± 0.09 for the NO_2 quantum yield, where the statistical uncertainty is two standard deviations.

Introduction

Peroxyacetyl nitrate or PAN, $CH_3C(O)OONO_2$, is a well known and important component of the atmosphere.[1] It was first detected in urban photochemical smog in the early 1960s. Subsequent field observations and laboratory studies have concluded that PAN is primarily formed *in situ* from reactions of NO_2 with oxidation products of small nonmethane hydrocarbons.[2] PAN has received much attention in the literature because it is a known eye irritant and phytotoxin in polluted urban air and serves as a long range transport vehicle of NO_X. PAN has been detected globally from ground level to 10 km altitudes at concentrations that are significant relative to the total NO_Y budget.[4-10] In the lower troposphere the concentration of PAN is controlled by thermal decomposition, which is strongly temperature dependent.[11-13] At higher altitudes PAN has a long thermal lifetime and other loss mechanisms become important. Because of the resistance of PAN to chemical attack by scavengers such as OH and Cl[14-17] and the stability against heterogeneous reaction,[18-20] photolysis is the dominant sink for PAN at altitudes greater than approximately 7 km.[17]

Although the ultraviolet absorption cross sections of PAN have been measured by several investigators with better than 10°/0 precision from 200 to 300 nm, [17,21,22] there are no experimental measurements of the product yields. Current data assessments employed in atmospheric models recommend only one PAN photolysis channel, [1,4] namely

$$PAN + h\nu \rightarrow CH_3C(O)OO + NO_2, \qquad \lambda_T = 9905240 \text{ nm} \quad (1a)$$

where the threshold wavelength is at 298 K. The low threshold for dissociation allows for the possibility of large amounts of internal energy disposal in the products. If the N02 product from channel 1a is sufficiently excited, it may undergo secondary dissociation, forming NO and O,

$$PAN + h\nu \rightarrow CH_3C(O)OO + NO + O(^3P) \qquad \lambda_T = 4854\text{-}55 \text{ nm} \quad (1b)$$

$$PAN + h\nu \rightarrow CH_3C(O)OO + NO + O(^1D). \qquad \lambda_T = 275 \pm 20 \text{ nm} \quad (1t)$$

Other energetically accessible channels for the ultraviolet photolysis of PAN can be proposed. One channel that is direct, and nearly iso-energetic with channel 1a, is

$$PAN + h\nu \rightarrow CH_3C(O)O + NO_3. \qquad \lambda_T = 1025 \pm 215 \text{ nm} \quad (2a)$$

The energy thresholds for the related reactions involving secondary dissociation of the NO_3 are

$$PAN + h\nu \rightarrow CH_3C(O)O + NO_2 + O(^3P) \qquad \lambda_T = 375 \pm 3011111 \quad (2b)$$

$$PAN + h\nu \rightarrow CH_3C(O)O + NO_2 + O(^1D). \qquad \lambda_T = 235 \pm 10 \text{ nm} \quad (2c)$$

PAN may also dissociate through concerted reactions, such as

$$PAN + h\nu \rightarrow CH_3 + CO2 + NO_3, \qquad \lambda_T = 1395 \pm 340 \text{ nm} \quad (3a)$$

$$PAN + h\nu \rightarrow CH_3 + CO2 + NO_2 + O(^3P), \qquad \lambda_T = 415 \pm 3011111 \quad (3b)$$

$$PAN + h\nu \rightarrow CH_3C(O)O + CO2 + NO_2 + O(^1D), \qquad \lambda_T = 250 \pm 1011111 \quad (3c)$$

or

$$PAN + h\nu \rightarrow CH_3C(O) + O2 + NO_2, \qquad \lambda_T = 445 \pm 35 \text{ nm} \quad (4a)$$

$$PAN + h\nu \rightarrow CH_3C(O) + O2 + NO + O(^3P), \qquad \lambda_T = 300 \pm 15 \text{ nm} \quad (4b)$$

$$PAN + h\nu \rightarrow CH_3C(O) + O2 + NO + O(^1D). \qquad \lambda_T = 205 \pm 511111 \quad (4c)$$

Several exothermic dissociation channels may also be conceived which require the rearrangement and breaking of several bonds. Examples include,

$$PAN \xrightarrow{h\nu} CH_3O + CO_2 + NO_2, \qquad \Delta H_{rxn} = -20 \pm 5 \text{ kcal/mol} \quad (5)$$

$$PAN \xrightarrow{h\nu} CH_3O_2 + CO_2 + NO, \qquad \Delta H_{rxn} = -6 \pm 5 \text{ kcal/mol} \quad (6)$$

where ΔH_{rxn} is at 298 K. The large uncertainties in the energetics of many of the above channels are a consequence of imprecision in the experimental heats of formation of $CH_3C(O)O$ (-52 ± 3 kcal/mol), $CH_3C(O)O_2$ (-4 1 ± 5 kcal/mol), and PAN (-62 ± 5 kcal/mol).[23-27]

Because PAN has a structureless ultraviolet absorption spectrum, one expects the photodissociation pathways to be direct: Consequently, channels 5, 6 and other mechanisms which require rearrangement of an excited intermediate prior to dissociation are not anticipated to be primary photolysis routes. In the Earth's atmosphere some of the photodissociation pathways lead effectively to the same products due to rapid secondary chemistry. For instance, the acetyl radical produced in channel 4 will rapidly combine with 02 to form the same organic product, peroxy acetyl radical, as obtained from channel 1. In addition, the unstable $CH_3C(O)O$ product of channel 2 will decompose into C02 and CH_3, yielding the same products as channel 3.[24] On account of these pathways, the atmospheric roles of the various photolytic channels reduce to two general possibilities. First, if the photodissociation is through channels 1 a or 4a, N02 and the peroxy acetyl radical are ultimately regenerated. Since PAN is largely formed in the atmosphere from the three body combination of these two products, this reaction pathway results in a chemical null cycle and the role of PAN at higher altitudes is solely as a reservoir and transport vehicle of nitrogen oxides. On the other hand, if the photolysis is through other channels, especially channel 2a, new chemical pathways arise which produce odd oxygen. In particular, the N03 formed will dissociate into N02 and O, either by solar photolysis or by unimolecular dissociation of the excited product, and the organic photoproducts will decompose to C02 and CH3. Since the

oxidation of the methyl radical also produces odd oxygen, both the organic and nitrogen containing photoproducts will affect the ozone budget.

In this work we have investigated NO_2 production from the photolysis of PAN at 248 nm. The N02 was detected by laser induced fluorescence (I .IF). By comparison to the $N0_2$ production from the photolysis of HNO_3 under identical experimental conditions, we have obtained a relative quantum yield for the production of NO_2. The implications of these results for atmospheric PAN chemistry will be discussed.

Experiment

A schematic of the experimental apparatus is shown in Fig 1. Gaseous samples of HNO_3 and PAN were introduced into the flowing system by passing a carrier gas (He, Ar, N_2, or 0_2) through a pyrex reservoir containing PAN or 1 HNO_3. in the case of HNO_3 the reservoir contained a neat solution of nitric acid, prepared by collecting the vacuum distillate of a 50:50 by volume mixture of 95% H_2SO_4 with $NaNO_3$. The 1 HNO_3 was maintained at 0°C by placing the sample in an ice bath.

The HNO_3 vapor concentration was determined by optical absorption at 254 nm in a 50 cm long absorption ccl] upstream of a teflon needle valve. The HNO_3 concentrations derived from the optical measurements agreed well with estimates based on the known vapor pressure of HNO_3. The pressure in the reservoir and absorption cell (25-150 '1'err) was controlled by a downstream needle valve and monitored with an MK S Baratron capacitance manometer. Al 1 flows rates were determined using calibrated flow meters.

The PAN samples were prepared by the method of Gaffney et al.[28] In accordance with this procedure the synthesized PAN was extracted from an acidic aqueous solution into *n*-tridecane ($C_{13}H_{28}$). The organic solution was then washed with 0°C water three times to remove water soluble impurities. The PAN vapor was introduced into the photolysis ccl] by

one of two methods. 'I'he organic solution was used directly as a source of gaseous PAN by transferring it to a reservoir and bubbling the buffer gas through the sample which was kept in a O°C icc bath. Because of the negligible vapor pressure of tridecane compared to PAN, this method provided essentially pure PAN in the gas phase. Fourier transform infrared spectra taken of the gaseous samples confirmed that the fraction of I'AN in the vapor was greater than 98%, in agreement with previous investigators.[28,29] For some trials, multiple samples Of pure PAN were collected by passing the vapor from the tridecane solution through a reservoir immersed in liquid nitrogen. The solid PAN, now containing only a trace amount of tridecane, was used as the sample for photolysis experiments. Appropriate precautions were taken in handling the pure PAN samples to protect against possible explosive decomposition. During photolysis experiments the pure PAN samples were maintained at a temperature of either -48°C using a *n*-hexanol slush or approximately -20°C using an aqueous $CaCl_2$ slush. The PAN was found to be quite stable at these temperatures. The advantages of the second operation were that 1) large quantities of PAN could be synthesized and collected at one time providing a longer lasting batch and 2) a more stable PAN vapor pressure was maintained compared to direct extraction from the tridecane. 130th methods yielded identical results within the experimental error.

The vapor pressure of the I'AN was determined by optical absorption through a 50 cm absorption cell. The 214 nm line of a Zn lamp was employed as the light source and the total pressure in the absorption cell was varied between 5 and 40 Torr. The optical cross sections for PAN have substantial more uncertainty as compared to 1 HNO_3. An average of experimental results from three independent studies was utilized to convert the absorbance to a concentration.1TY21 ,[22] As wi 11 be discussed further in the *Uncertainty Analysis* part of the Results section, the magnitude of the absolute concentrations of PAN will vary, depending on which experimental sets of cross sections arc utilized, however, the measured relative quantum yield of N02 production is very independent to which data set is employed in the analysis. As an additional test to confirm our ability to accurately measure the concentration

of PAN, absorption measurements were also made at 254 mm, The calculated concentrations at the two wavelengths agreed we] 1, however, the 214 nm determinat ion was preferred because the optical density of the PAN at this wavelength closely matched that of the HNO_3 at 254 nm using the same absorption cell path length.

The concentrations of the gases in the quartz photolysis cell were reduced relative to those in the upstream absorption ccl] by injection of additional buffer gas in a mixing manifold located between the cells. The concentration of 1 HNO_3 in the photolysis cell ranged between (O. 1 -45.0) x 10^{14} cm^{-3} and that of PAN was varied between (0.5-5.0) x 10^{14} cm^{-3}. In all experiments, the partial pressures of the precursors were maintained low enough that the fluorescence quenching was controlled solely by the carrier gas.[30] The optical densities of PAN to HNO_3 in the photolysis cell were maintained within approximately an order of magnitude of each other. The total pressures in the photolysis cell ranged from 1 to 16 Torr. Depending on total pressure, the flow rate into the cell was maintained between 250 to 4000 seem which was adequate to remove photoproducts from the detector viewing zone between photolysis laser shots.

The weakly focused output of an excimer laser (Questek Model 2240) operating at 248 nm and at a pulse repetition rate of 30 Hz was used to photolyze the precursors. The energy density ranged from 35 to 75 mJ/cm^2 per pulse and was monitored with a Joule meter (Scientech P50). Under these conditions the photolytic signal was observed to be linear with laser pulse energy. Typically 25,000-50,000 laser shots were averaged for one experiment.

A pulsed copper vapor laser (W].: Oxford model CU 15A) operating at a tunable repetition rate between 10 to 20 kHz was utilized for LIF detection of NO_2. The 578 nm output from the CVL was eliminated by passage of the beam through two short wavelength pass filters. The transmitted 511 nm line was directed through a telescope to reduce the diameter of the beam to approximately 0.5 cm. The weakly convergent beam was then sent to the photolysis cell.

The LIF signal was detected by a cooled photomultiplier tube (PMT: Burle C3 1034-02) that was oriented perpendicular to the laser beam axes, The LIF signal was amplified, discriminated, and counted on a multi-channel scaler card (MCS: Canberra Accuspec) configured with bin widths of either 5 or 10 ps. A 550 nm long pass filter was placed in front of the I'MI' to block excimer and CVI, laser scatter, An LIF detection sensitivity of approximately 3×10^9 $NO_2 cm^{-3}$ was achieved with signal averaging of 25,000 CVL pulses.

The timing and synchronization of the two lasers were controlled by a high frequency master clock (10-20 kHz), a frequency divider circuit, and two delay generators. The master clock pulses were used to trigger the CVL and the appropriately delayed low frequency (30 Hz) outputs of the frequency divider were used to trigger the excimer and the MCS data collection. This arrangement allowed for selection of a wide range of delay times between the excimer laser pulse, the copper vapor laser pulse, and the signal collection.

Results

Experimental observations

Fluorescence data following photolysis of PAN and 1 HNO_3 were collected at total pressures from 1 to 16 Torr in four different carrier gases; 1 Ic, Ar, N_2, and 0_2. The high repetition frequency of the probe laser resulted in acquisition of' an LIF data point every 50 to 100 μs, depending on selected WI, repetition rate. The rapid temporal sampling of the NO_2 produced very well resolved profiles of N02 loss (i.e. diffusion and flow) from the viewing zone. In Fig 2A raw data from HNO_3 photol ysis in 3.5 Torr of Ar are shown. The probe laser was operating at 10 k] Iz and LIF signal is clearly seen above the more rapidly decaying background noise, which originates from cell and filter fluorescence induced by the excimer laser. The background noise was removed from the data and the residual LIF signal from the probe laser is shown in Fig 211. The line in Fig 2B is a 4th order polynomial regression to

guide the eye, The temporal profile of the probe signal was analyzed until the NO_2 photoproduct completely left the detection viewing zone at which time the LIF signal was constant and finite due to background $N0_2$ from slight decomposition of the I $IN0_3$ sample and leakage of the laser light through the filters. The background probe signal was removed from the data to obtain the actual signal from photolysis. The error bars in Fig 2 represent the shot noise of the data.

Under otherwise identical experimental conditions, the loss rates of the LIF signals generated from PAN and 1 INO_3 were the same This is illustrated in Fig 3A, where all sources of background signal have been removed from the data, in order to determine the relative production of $N0_2$ from each of the precursors, absolute signals from each, at set delays bet wccn pump and probe pulses, were ratioed, as shown in Fig 3B, and an average of these independent values yielded the relative yield of N02. The normalization of this average to the initial optical densities of the precursors converts this quantity to a relative quantum yield. Details arc presented in the next section. Typical 1 y, data were averaged from the first probe pulse after the photolysis, $t \leq 50$ μs, to approximately 1500 μs after the photolysis to determine the average relative signal. Because of the rapid loss of the N02 photoproducts at early time, the "point by point" analysis, shown in Fig 3B, results in better precision than an analysis based on extrapolating the LIF temporal profile back to the time of the pump pulse and comparing the calculated nascent signals.

The best LIF signal to noise ratios were obtained with Ar as a carrier, due to its less efficient fluorescence quenching compared to 0_2 and N_2. Although Helium has an electronic quenching rate coefficient similar to Argon[30], its diffusion rate is nearly 4 times as great.q [1] The rapid diffusion characteristic limited the temporal range over which useful LIF data could be obtained in He, except at higher total pressures, i.e. > 10 '1'err, where increased fluorescence quenching became the major limitation in all the buffer gases.

Our previous investigations of HNO_3 photolysis revealed that the nascent N02 produced from HNO_3 is internally excited.[32] Based on observations of the early time profile

of the fluorescence from PAN, we also conclude that the majority of the nascent NO_2 from PAN photolysis is also electronically excited. At total pressures below 3 Torr, this excitation complicated the early time interpretation of the LIF signal in all of the buffer gases except for O_2 whose vibrational collisional quenching of NO_2 is markedly more efficient.[32] This internal excitation, combined with faster diffusional loss of the NO_2, hindered data acquisition at the lower pressures. A consideration of effects associated with diffusion, fluorescence quenching, and collisional deactivation of the hot nascent NO_2 indicated that the maximum signal to noise ratio was achieved at a total pressure of approximately 7 Torr. Consequently, the majority of the data was taken at this pressure.

Quantum Yield Determination Methodology

The nascent NO_2 concentration, $[NO_2]$, produced from monochromatic photolysis of a precursor gas, i, may be expressed by the following

$$[NO_2]_i = A\ \phi_i^{NO_2}(\lambda_{photo})\ [i]\ \sigma_i(\lambda_{photo}) \qquad (7)$$

where λ_{photo} is the photolysis wavelength. The NO_2 quantum yield, $\phi_i^{NO_2}$, is defined as the ratio of the total number of NO_2 molecules produced relative to the number of photons absorbed by the precursor, i, which has an initial concentration, $[i]$, and optical cross section, $\sigma_i(\lambda_{photo})$. The quantity A is a detection response function and depends on the energies of both the pump and probe lasers, the photon detection geometry, and, in the case of fluorescence detection, the extent of collisional quenching. The direct determination of A is, in general, very difficult, largely due to the spatial inhomogeneities of the energy in the laser beams. For this reason, a relative measurement scheme was utilized in order to determine the quantum yield of NO_2 production from PAN photolysis.

The photolysis of a reference gas whose optical cross section and NO_2 quantum yield are known may be employed as a calibrant in determining the quantum yield of the molecule of interest. By measuring the relative NO_2 production from these two species, under otherwise identical experimental conditions, the quantum yield for the gas under study is

obtained without the direct need for knowledge of A. The photolysis of 1 $IN0_3$ was chosen as a calibrant to determine the quantum yield of NO_2 from PAN. The relative NO_2 concentrations produced from each of the experiments is related to the quantum yield by the following expression

$$\frac{[NO_2]_{PAN}}{[NO_2]_{HNO_3}} = \frac{S_{PAN}(\tau)}{S_{HNO_3}(\tau)} = \frac{\phi_{PAN}^{NO_2}(\lambda_{photo})}{\phi_{HNO_3}^{NO_2}(\lambda_{photo})} \frac{[PAN]}{[HNO_3]} \frac{\sigma_{PAN}(\lambda_{photo})}{\sigma_{HNO_3}(\lambda_{photo})} \quad (8)$$

where A has now been eliminated by ratioing the two. In Eq 8, $S_i(\tau)$ is the fluorescence signal from each precursor at time, τ, after photo] ysis. Rearrangement gives

$$\phi_{PAN}^{NO_2}(\lambda_{photo}) = \phi_{HNO_3}^{NO_2}(\lambda_{photo}) \frac{S_{PAN}(\tau)}{S_{HNO_3}(\tau)} \frac{[HNO_3]}{[PAN]} \frac{\sigma_{HNO_3}(\lambda_{photo})}{\sigma_{PAN}(\lambda_{photo})} . \quad (9)$$

Eq 9 is the fundamental equation to convert the raw data to a quantum yield. In Eq 9 the experimental observable arc the relative concentrations and the relative signals. If these quantities are plotted against one another the slope is proportional to the relative quantum yield, An example of this analysis is shown is Fig 4, where each data point was obtained by the analysis illustrated in Fig 3. In order to convert this slope into a relative quantum yield, the optical cross sections of each precursor at both the photolysis and, in the present case, absorption wavelengths must be known.

Uncertainty Analysis

The ultraviolet optical cross sections for PAN have been independently measured by several investigators. Senum *et al.*[21] recorded the absorption spectrum from 200 to 300 nm and values were tabulated every 5 nm with an assigned uncertainty of *8°/0,* An interpolated fit of their data yields values of (12.0 ± 1.0) x 10-20 cm^2 molecule^{-1} and (123 ± 10) x 10-20 cm^2 molecule^{-1} at 248 nm and 214 nm, respectively, which arc the wavelengths employed in the present study for photolysis and concentration determination by absorption. Slightly larger magnitudes at these two wavelengths have been obtained recently by Talukdar *et al.*,[17] (1 4.6

± 0.7) × 10^{-20} cm^2 $molecule^{-1}$ and (143 ± 7) × 10^{-20} cm^2 $molecule^{-1}$, and Libuda and Zabel,[22] 14.6 x 10^{-20} cm^2 $molecule^{-1}$ and 145 x 10-20 cm^2 $molecule^{-1}$ (uncertainties for these values were not reported). Although the magnitude of the absolute cross sections differ between the earlier work of Senum et al. and the two more recent observations, the values of the relative cross sections agree well: the ratios of the reported cross section at 214 nm to that at 248 nm are 10.2 ± 1.2, 9.8 ± 0.7, and 9.9 for the results of Senum *et* al., Talukdar *et* al., and Libuda and Zabel, respectively. The accuracy of the relative measurements likely exceed those of the absolute ones because systematic uncertainties cancel. The average of the three cross sectional data sets is

$$\frac{\sigma_{PAN}(\lambda_{abs} = 214nm)}{\sigma_{PAN}(\lambda_{photo} = 248nm)} = 10.0 \pm 0.4, \qquad (10)$$

where the uncertainty is two standard deviations in the average of the three data sets and the subscripts *abs* and *photo* refer to the absorption and photolysis wavelength, respectively.

In the present studies the initial precursor concentrations were obtained by measuring the optical absorbance at a particular absorption wavelength, $A(\lambda_{abs})$, i.e.

$$A_i(\lambda_{abs}) = \sigma_i(\lambda_{abs})\, L\, [i], \qquad (11)$$

where L is the cell path length. Replacing the concentration terms in Eq 9 with the actual observable, the absorbance, yields

$$\phi_{PAN}^{NO_2}(\lambda_{photo}) = \phi_{HNO_3}^{NO_2}(\lambda_{photo}) \frac{S_{PAN}(\tau)}{S_{HNO_3}(\tau)} \frac{A_{HNO_3}(\lambda_{abs})}{A_{PAN}(\lambda^*_{abs})} \times \frac{\sigma_{PAN}(\lambda^*_{abs})}{\sigma_{PAN}(\lambda_{photo})} \frac{\sigma_{HNO_3}(\lambda_{photo})}{\sigma_{HNO_3}(\lambda_{abs})}. \qquad (12)$$

Because the same absorption cell was employed in the measurement of the absorbance of each precursor, the cell path length cancels out of the expression. The use of different absorption wavelengths for PAN and HNO_3 are distinguished by an asterisk in Eq 12.

The absorption cross sections are better established for HNO_3 than for PAN. The results of Johnston and Graham[33], Biaume[34], and Molina and Molina[35] all agree well at 248

and 254 nm. Biaume reported cross sections of 1.98×10^{-20} cm^2 molecule^{-1} and 1.95×10^{-20} cm^2 molecule- I at the Hg lines at 248.48 and 253.65 nm, respectively. These values was used for the analysis of our data. The estimated error of the 11N03 cross sections at these wavelengths is 1 %. These values result in the following ratio, where the uncertainty is two standard deviations,

$$\frac{\sigma_{HNO_3}(\lambda_{photo})}{\sigma_{HNO_3}(\lambda_{abs})} = 102 \pm 0.03 \quad (13)$$

incorporating Eqs 10 and 13 into Eq 12 yields

$$\phi_{PAN}^{NO_2}(\lambda_{photo}) = (10.2 \pm 0.5) \times \phi_{HNO_3}^{NO}(\lambda_{photo}) \frac{S_{PAN}(\tau)}{S_{HNO_3}(\tau)} \frac{A_{HNO_3}(\lambda_{abs})}{A_{PAN}(\lambda^*_{abs})}. \quad (14)$$

The relative quantum yield from the photolyses of PAN and I $IN0_3$ has now been put into a functional form which is dependent on the experimental observable. The only remaining scaling quantity to convert the data to an absolute yield is $\phi_{HNO_3}^{NO_2}(\lambda_{photo})$.

The photolysis of I $IN0_3$ has been studied at a variety of wavelengths .sc^{-1} At a photolysis wavelength of 248 nm the following four channels are energetically allowed

$$HNO_3 + hv \rightarrow NO_2 + 011, \quad \lambda_T \leq 60111111 \quad (15)$$

$$\rightarrow O(31') + HONO, \quad \lambda_T \leq 40011111 \quad (16)$$

$$\rightarrow H(^2S) + NO_3, \quad \lambda_T \leq 286 \text{ nm} \quad (17)$$

$$\rightarrow 11(2S) + NO + O_2, \quad \lambda_T \leq 278 \text{ nm} \quad (18)$$

where the threshold wavelengths are given at O K. No I I atom production has been detected from HNO_3 photolysis over the wavelength range from 193 to 266 nm,[36,37] indicating that both channels 17 and 18 arc insignificant dissociation pathways at 248 nm, however, channels 15 and 16 are both active ultraviolet photolysis channels for HNO_3 with branching ratios that arc strongly wavelength dependent. In the recent work of Turnipseed *et al.*[37], which emplo yed a relative quantum yield determination scheme similar to the present approach for PAN, values of $\phi_{HNO_3}^{OH}$ (and $\phi_{HNO_3}^{O}$) were reported to be 0.95 ± 0.06 (0.031 ± 0.009), 0.90+-0.11 (0.20 ± 0.03), and 0.33 ± 0.09 (0.81 ± 0.13) at 248, 222, and 193 nm, respectively.

Schiffman *et al.*,[41] also observed a decrease in $\phi^{OH}_{HNO_3}$ at lower photol ysis wavelengths, obtaining values of 0.75 ± 0.10 and 0.47 ± 0.06 at 248 and 193 nm, respectively.

Using stable end product analysis, Johnston *et al.*[38] concluded that the quantum yield of channel 15 is unity over the wavelength range 200 to 300 nm. Also, in a direct quantum yield determination, Jolly *et al.*[39] measured $\phi^{OH}_{HNO_3}(222\ \text{nm}) = 0.89 \pm 0.08$. Taken together, these investigations indicate that the lowest energy photodissociation pathway, channel 15, is the dominant pathway at 248 nm and channel 16 becomes important possibly at 222 nm and certainly by 193 nm. Except for the results of Schiffman *et al.*[41], these studies also suggest $\phi^{OH}_{HNO_3}(248\ \text{nm}) = 1$, Since at 248 nm there is insufficient energy for the N02 from channel 15 to dissociate and channel 15 is the only energetically available route to give rise to OH, the quantum yield of OH from HNO_3 at 248 nm, $\phi^{OH}_{HNO_3}$ (248 nm), is equivalent to $\phi^{NO_2}_{HNO_3}$ 248 nm).

in the analysis of the present data we assume, based on the majority of the literature results, a unity quantum yield for channel 15 at 248 nm. The retrieved quantum yield from PAN is, therefore, an upper limit to the actual value. Future refinements in the HNO_3 quantum yield values will require appropriate scaling of the PAN results, The summary of data obtained over a range of total pressures, carrier gases, and concentrations of PAN is shown in Table 1. A variance weighted average of the relative product yields listed in Table 1 is 0.83 ± 0.08, where the quoted uncertainty is two standard deviations in data precision. When the uncertainties in the ratio of the PAN optical cross sections at the absorption and photolysis wavelengths are incorporated into the result the error increases slightly to ± 0.09.

Discussion

In the analysis of our data wc have assumed a unity quantum yield for production of N02 from HN03 photolysis at 248 nm. This assumption is supported by results of several previous investigations. I Iowever, recent results of Schiffman *et* a/.[4] point to a significantly lower quantum yield. Employment of these latter results would substantially lower our calculated $\phi_{PAN}^{NO_2}$ (248 nm) to a value of 0.62 ± 0.11, As an internal test, wc conducted a few photolysis experiments with $ClONO_2$. over the pressure range from 1 to 8 Torr in Ar and compared the signal strengths with 11N03 photolysis data taken under the same conditions. Referencing the relative signals to the recently published literature value of $\phi_{ClONO_2}^{NO_2}$ (^{248} nm)[42] leads ‘0 better consistency ‘f $\phi_{HNO_3}^{NO_2}$ (^{248} nm) ‘s assumed ‘0 be unity rather than 0.75, as reported by Schiffmann *et al.*. Consequently, these conclusions support the results of Turnipseed *et al.*[37] and others[38,39] which imply a unit quantum yield of N02 from HNO_3 photolysis at 248 nm. 1 lowever, the $ClONO_2$ photochemical system is complex and further quantitative measurements of I IN03 photolysis products are warranted in order to resolve this discrepancy.

The analysis of the present data suggests that N02 is the major nitrogen-containing product from PAN photolysis at 248 nm, however, because of large experimental uncertainties wc cannot preclude the possibility of other nitrogen containing photoproducts, such as NO_3 from a direct mechanism (channels 2a or 3a) or NO formed from the secondary dissociation of internally excited N02 (channels 1 b, 1 c, or 4b). The mechanism(s) for N02 generation from 248 nm PAN photolysis can be direct (channels 1a or 4a) and/or indirect from secondary dissociation of NO_3 (channels 2b, 3b, or 3c). Although the present data cannot unambiguously resolve which of these channels give rise to the N02, we consider channels 1 a and 4a, where one and two bonds arc broken, respectively, to be the most likely photolysis pathways. Both 1a and 4a arc expected to produce the same atmospheric effect, because the

acetyl radical produced in 4a will rapidly recombine with molecular oxygen to form peroxy acetyl radical which is the organic product of 1a. Moreover, the formation of NO_2 as the nitrogen-containing photoproduct of these reaction channels represents a net chemical null cycle for PAN. Consequently, the major role of I'AN in the stratosphere and upper troposphere is as a long range transport vehicle for N02.

We consider other N02 forming mechanisms to be unlikely. Production of N02 from the secondary dissociation of the NO_3 product from channels 2 and 3 requires that the NO_3 be substantially internally excited. This requirement is not simultaneously compatible with our finding that the N02 product from PAN photolysis at 248 nm contains a significant amount of' internal energy. In order for the NO_2 to be electronically excited, as is observed, it must have energy in excess of approximately 10,000 cm^{-1}.[30] The lower limit of the total energy necessary to form electronically excited N02 by channels 2b and 3b is 105 kcal/mol and 97.8 kcal/mol, respectively. Since the energy of the 248 nm photon is 115.3 kcal/mol, this leave.s less than 20 kcal/mol of energy available for internal excitation of the other photoproducts and for product translational energy. An investigation of the photolysis of methyl nitrate at 248 nm, a molecule similar to PAN, has shown that an average of 23 kcal/mol is deposited into product translational energy and between 47 to 72 kcal/mol of energy is in the internal energy of the photoproducts.[43] Similar energy disposal was observed in the photolysis of chlorine nitrate, another closely related molecule.[42] Based on these results we conclude on energetic grounds that the N02 is being produced directly from either channel 1 a or 4a and N02 production from secondary dissociation of NO_3 is highly unlikely.

Acknowledgments

The research described in this paper was carried out at the Jet Propulsion Laboratory, California Institute of Technology, under contract with the National Aeronautics and Space Administration.

References

(1) Kleindienst, T.E. *Res. Chem. Intermed.* **1994**, 20,335, and references within.

(2) Aikin, A. C.; Herman, J. R.; Maier, E. J. R.; McQuillan, C. *J. Planet. Space Sci.* 1983,31, 1075.

(3) Singh, H. D.; Salas, L. J.; Viezee, W. *Nature* 1986,321,588.

(4) Kasting J. F.; Singh, H.B. *J. Geophys. Res.* 1986,91, 13239.

(5) Shepson, P. B.; Hastie, D. R.; So K. W.; Schiff, H. I. *Atmos. Environ.* 1992, *26A*, 1259.

(6) Derwent, R. G.; Jenkin, M. E. *Atmos. Environ.* **1991,** 25A, 1661.

(7) Kasibhatla, P. S.; Levy, H., II; Moxim, W. J. *J. Geophys. Res.* 1993,98,7165.

(8) Honrath, R. E.; Jaffe, D. A. *J. Geophys. Res.* 1992, 97, 20615.

(9) Singh, H. B.; O'Hara, D.; Herlth, D.; Bradshaw, J. D.; Sandholm, S. T.; Gregory, G. L.; Sachse, G. W.; Blake, D. R.; Crutzen, P. J.; Kanakidou, M. A. *J. Geophys. Res. 1992,* 97, 16511.

(10) Parrish, D. D.; Hahn, C. J.; Williams, E. J.; Norton, R. B.; Fehsenfeld, F. C.; Singh, H. B.; Shetter, J. D.; Gandrud, B. W.; Ridley, B. A. *J. Geophys. Res.* 1992, 97, 15883.

(11) Orlando, J. J.; Tyndall, G. S.; Calvert, J. G.; *Atmos. Environ.* 1992, 26A, 3089

(12) Roberts, J. M.; Bertman, S. B. *Int. J. Chem. Kinetics* **1992, 24, 297**

(13) Grosjean, D; Grosjean, E.; Williams, E. L., II J. *Air& Waste Manage. Assoc.* 1994,44, 391.

(14) Wellington, T. J.; Atkinson, R.; Winer, A. M. *Geophys. Res. Lett.* 1984, 11,861

(15) Tsalkani, N.; Mellouki, A.; Poulet, G.; Toupance, G.; Le Bras, G. *J. Atmos. Chem. 1988, 7,409.*

(16) Wellington, 'l'. J.; Andino, J. M.; Ball, J. C,;Japar, S. M. *J. Atmos. Chem. 1990,10,301.*

(17) Talukdar, R. K.; Burkholder, J. B.; Schmoltner, A. -M.; Roberts, J. M.; Wilson, R.; Ravishankara, A. R. *manuscript in preparation.*

(18)1101drcn, M. W.; Spicer, C. W.; Hales, J. M. *A/trios. Environ.* 1984,18,1171,

(19) Moore, S. 13.; Friedl, R. R.; Sander, S. P. *manuscript in preparation,*

(20) Langer, S.; Wängberg, 1.; Ljungström, E. *Atmos. Environ. 1992, 26A, 3089.*

(21) Senum, G. I.; lee, Y. -N.; Gaffney, J. S. *J. Phys. Chem.* 1984,88, *1269.*

(22) Libuda, 1-1. G.; Zabel, F. *Paper presented at XXIst Informal Conference on Photochemistry,* Toronto, May 1994.

(23) Sicilia, E.; Di Maio, F. P.; Russo, N. *J. Phys. Chem. 1993,97,528.*

(24) Bridier, 1.; Caralp, F.; Loirat, H.; Lesclaux, B. V.; Veyret, B.; Becker, K. 11.; Reimer, A.; Zabel, F. *J. Phys. Chem. 1991, 9.5,3594.*

(25) 1 Iolmes, J. L.; Lossing, F. 1'.; Mayer, P. M. *J. Am. Chem. Soc.* 1991, 113,9723.

(26) Hendry, D. G.; Kenley, R. A. *J. Am. Chem. Soc.* 1977,99,3198.

(27) DeMore, W. B.; Sander, S. P.; Golden, D. M.; 1 Iampson, R. F.; Kurylo, M. J.; 1 Ioward, C. J.; Ravishankara, A. R.; Kolb, C. E.; Molina, M. J. *JPL Publication 92-20;* Jet Propulsion laboratory: Pasadena, CA, 1992.

(28) Gaffncy, J. S.; Fajer, R.; Senum, G. 1. *Atmos. Environ. 1984, 16',215.*

(29) Bruckmann, P. W.; Willner, I I. *Environ. Sci. Technol. 1983, 17,352.*

(30) Okabe, H *Photochemistry of Small Molecules*; John-Wiley and Sons: New York, 1978,

(31) Marrero, T. R.; Mason, E. A, *J. Phys. Chem. Ref. Data 1972,1,3.*

(32) Mazely, T. L.; Friedl, R. R.; Sander, S. P. J. *Chem. Phys.* 1994, 100,8040.

(33) Johnston, H. S.; Graham, R. *J. Phys. Chem. 1973, 77,62.*

(34) Biaume, F. *J. Photochem. 1973,2,* 139.

(35) Molina, L. T.; Molina, M. J. *J. Photochem. 1981, 15,97.*

(36) Margitan, J. J,; Watson, R. '1'. *J. Phys. Chem. 1982,86,3819.*

(37) Turnipseed, A, A.; Vaghjiani, G. 1,.; Thompson, J. 1.; Ravishankara, A. R. *J. Chem. Phys.* 1992,96,5887.

(38) Johnston, H. S,; Chang, S-G; Whitten, G. J. *Phys. Chem.* 1974, *78,* 1

(39) Jolly, G, S,; Singleton, D. L.; McKenney, D. J.; Paraskevopoulos, G. J. *Chem. Phys.* 1986,84,6662.

(40) Kenner, R. D.; Rohrer, F.; Papenbrock, Th.; Stuhl F., *J. Phys. Chem.* 1986,90,1294.

(41) Schiffman, A,; Nelson, D. D., Jr.; Nesbitt, D. J. *J. Chem. Phys.* 1993,98,6935.

(42) Minton, T. K.; Nelson, C. M.; Moore, '1'. A.; Okumura, M. *Science 1992,256',* 1342.

(43) Yang, X.; l'elder, P.; Huber, J. R. *J. Phys. Chem.* 1993,97, 10903.

Table 1

P, Torr	M	Φ_{NO_2}	HNO_3 lulls	PAN runs	[PAN] x 10^{13} cm^{-3}
1	O_2	*0.90 ± 0.25*	1	1	*4.5*
3	Ar	0,84 ± 0.08	4	4	8,0-29.3
4	O_2	0.75 ± 0.22	6	6	2.6-25.8
7	O_2	0.75 ± 0.15	1	1	31.6
7	Ar	0.84 ± 0.09	3	4	6.8-11.3
7	N_2	0.80 ± 0.20	2	2	2,1-45.1
16	He	0,90 ± 0.20	1	1	14.4

Figure Captions

Figure 1: Schematic of the experimental apparatus.

Figure 2: A) Raw data from the photolysis of 2.9 x 101 ^{5} HNO_3 cm^{-3} in 3.5 Torr of Ar. The signal from 16,000 excimer shots was summed to obtain this temporal profile. The densely spaced lower trace is from ccl] and filter fluorescence induced by the excimer. The upper trace is LIF from the probe laser superimposed on the background noise. B) The background noise from the excimer is removed from the data in part A. The residual signal is the LIF solely due to the probe laser. The signal is consists of three components; 1) NO_2 generated from HNO_3 photo] ysis, 2) NO_2 from slight HNO_3 decomposition, and 3) probe laser scatter through the optical filters.

Figure 3: A) N02 LIF signal vs. time is shown for photolysis of similar optical densities of I'AN (3.2 x 10^{14} cm^{-3}) and HNO_3 (1.0 x 10^{15} cm^{-3}) in 7 Torr of O_2. The decay of the signal is largely due to diffusion. Solid lines through the data arc biexponential fits to the data which provide a visual guide. B) Relative signal strengths of NO_2 fluorescence from PAN and 1 HNO_3. The average of the relative signal from data taken between O and 1400 μs after the excimer pulse is 1.50 ± 0,30, where the error bar is two standard deviations in experimental precision. The employment of Eq 9 converts the signal ratio to a quantum yield of 0.75 ± 0.15.

Figure 4: The relative fluorescent signals of NO_2 from PAN and HNO_3 photolyses at 248 nm in 7 Torr of Ar as a function of the corresponding relative concentrations of each precursor Each data point represents a temporally averaged ratio of LIF signal, similar to those illustrated in Fig 2A. The slope of the solid line is proportions] to $\phi_{PAN}^{NO_2}$. The value obtained

from this plot for the quantum yield is 0.84 ± 0.09, where the error is two standard deviations in data precision.

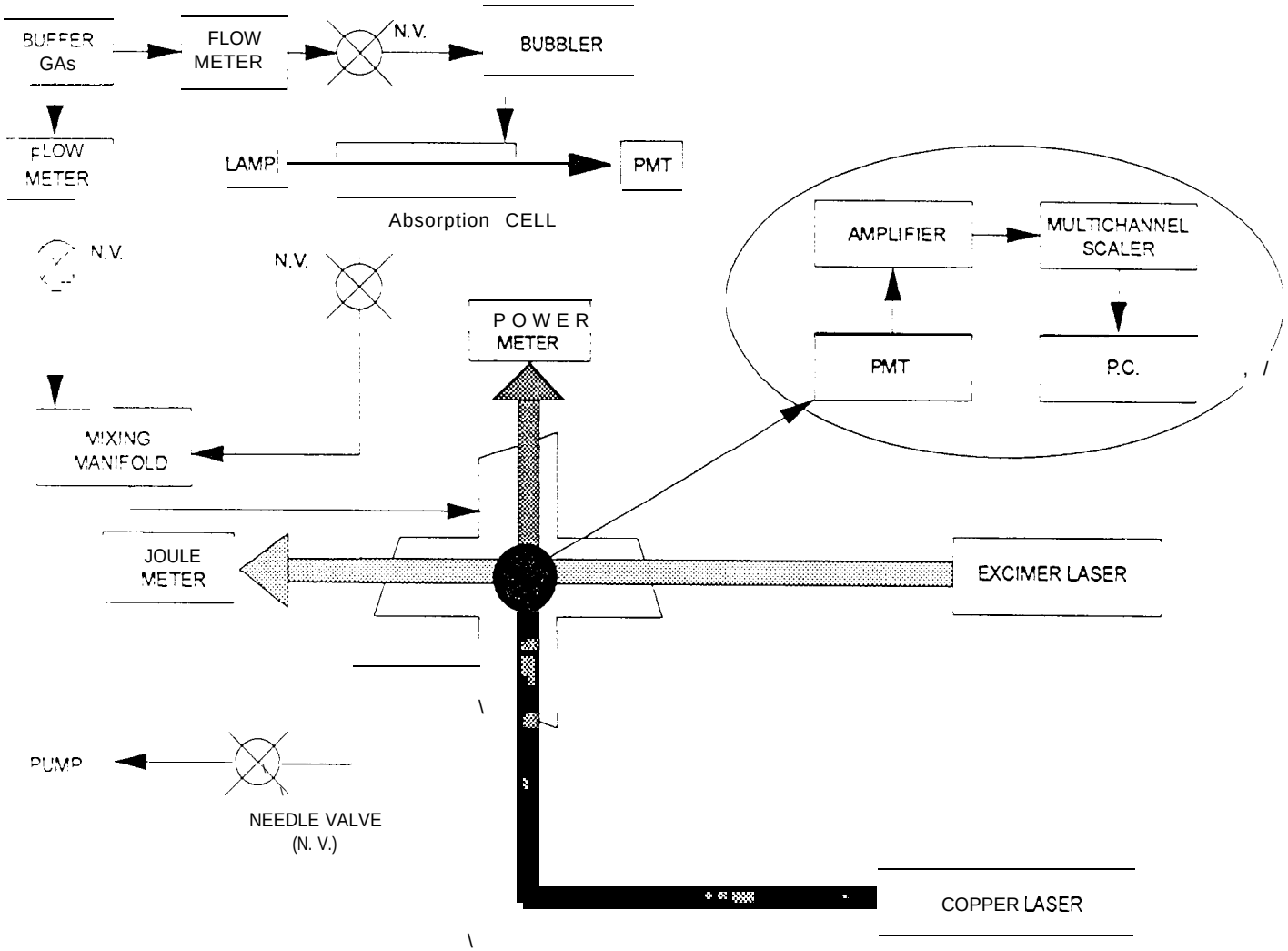
BUFFER GAs
FLOW METER
N.V.
BUBBLER
FLOW METER
LAMP
PMT
Absorption CELL
N.V.
N.V.
POWER METER
AMPLIFIER
MULTICHANNEL SCALER
PMT
P.C.
MIXING MANIFOLD
JOULE METER
EXCIMER LASER
PUMP
NEEDLE VALVE
(N. V.)
COPPER LASER

Fig 1

Fig. 2

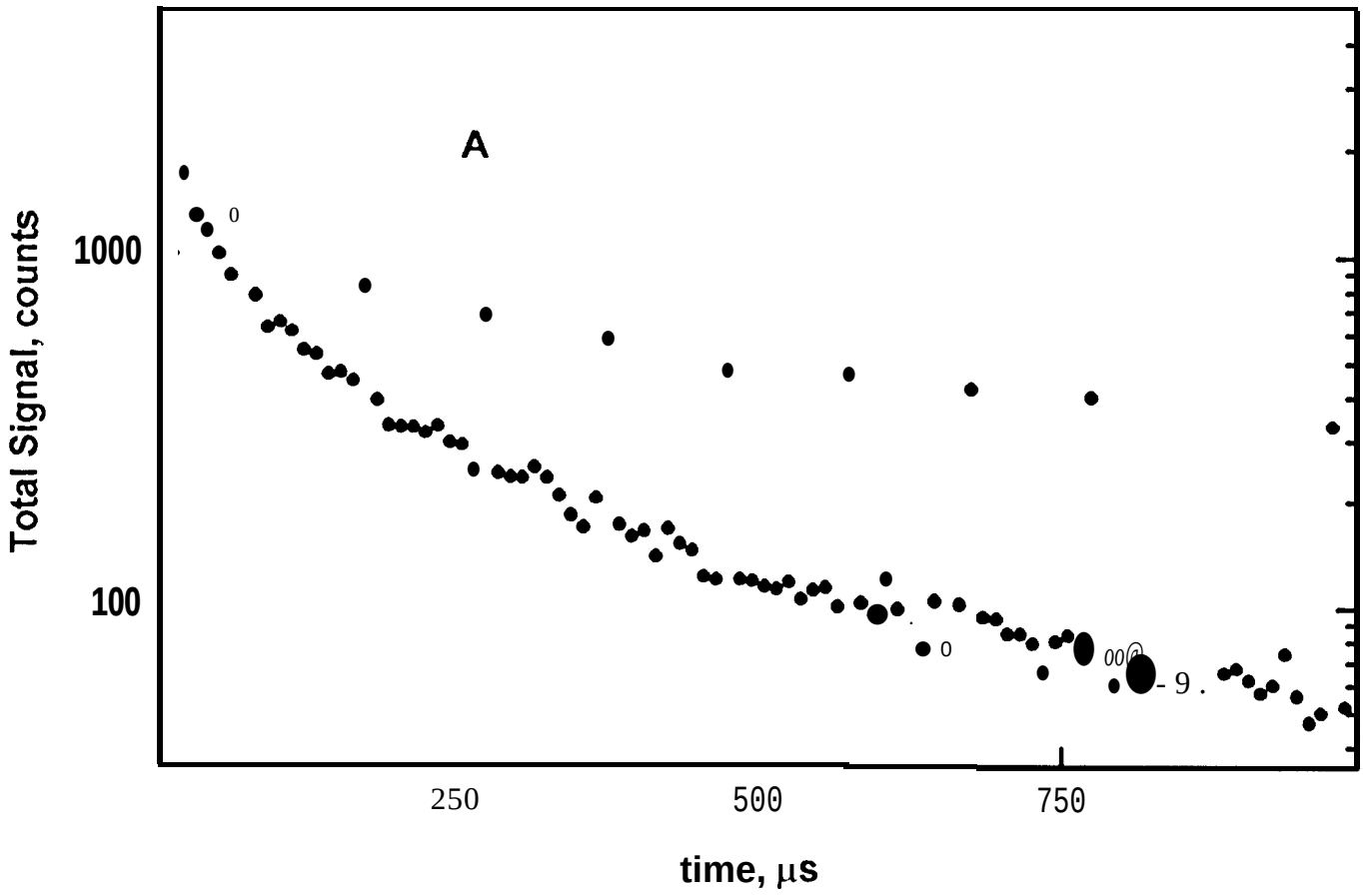
A
Total Signal, counts
1000
100
250
500
750
time, μs

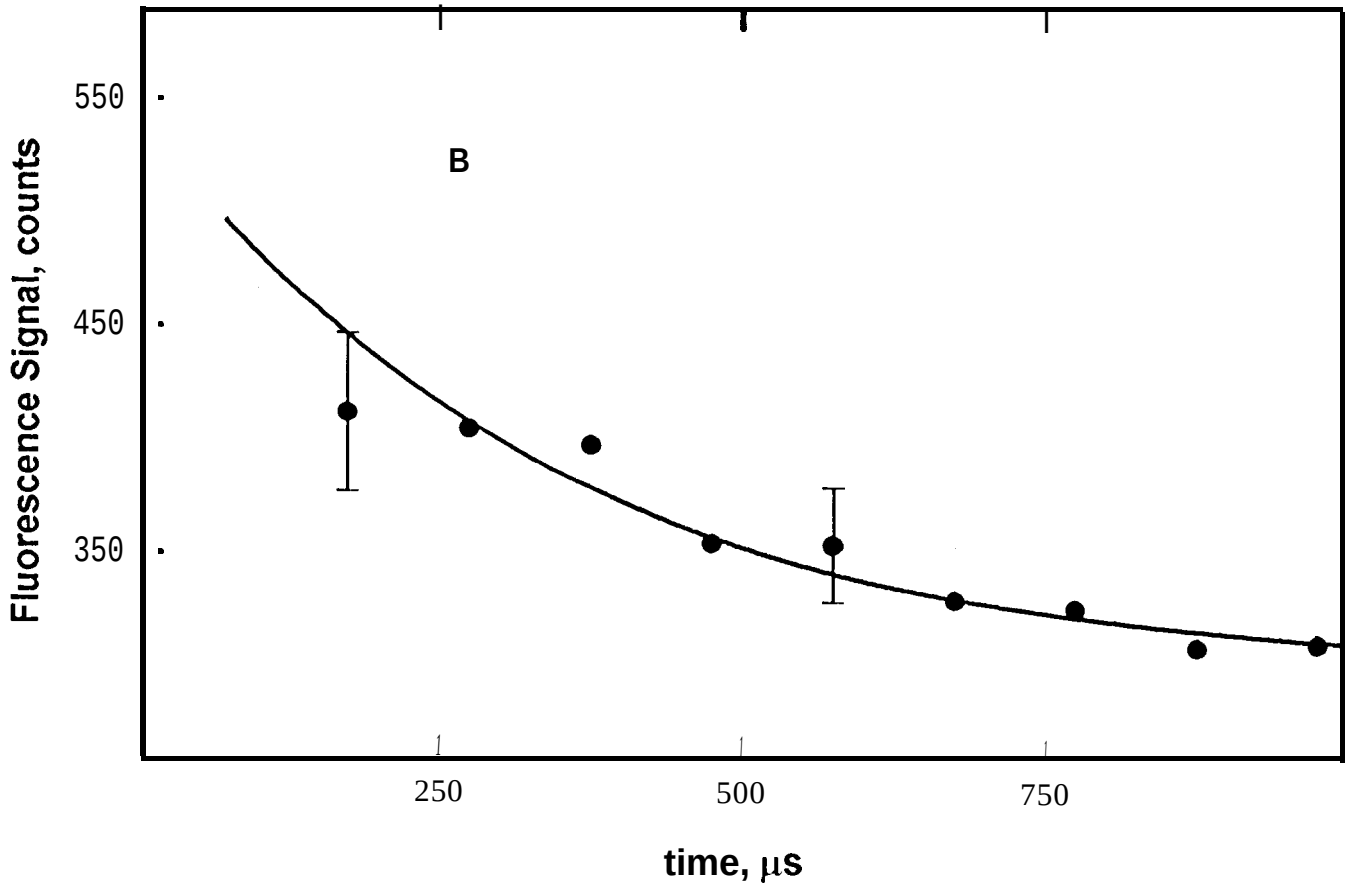
B
Fluorescence Signal, counts
550
450
350
250
500
750
time, μs

Fig. 3

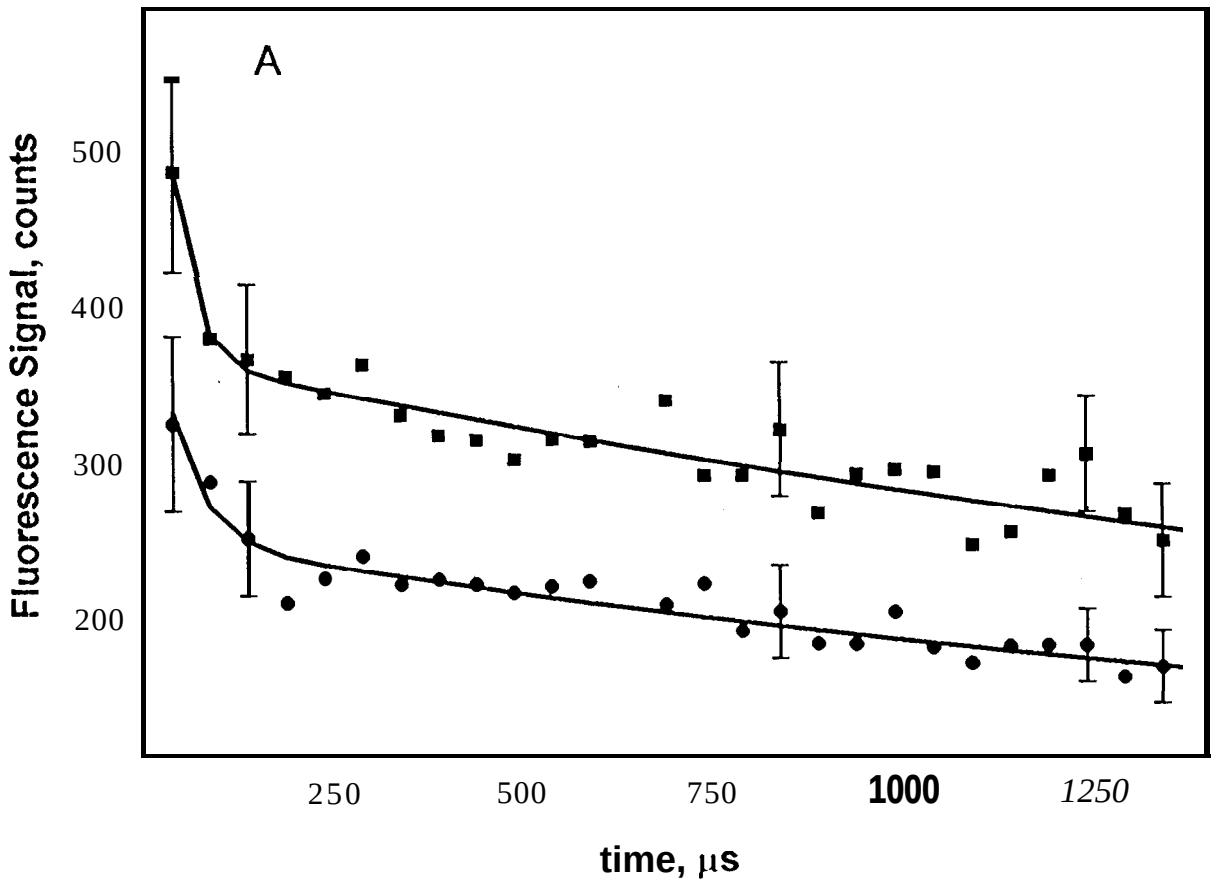
A
Fluorescence Signal, counts
500
400
300
200
250
500
750
1000
1250
time, μs

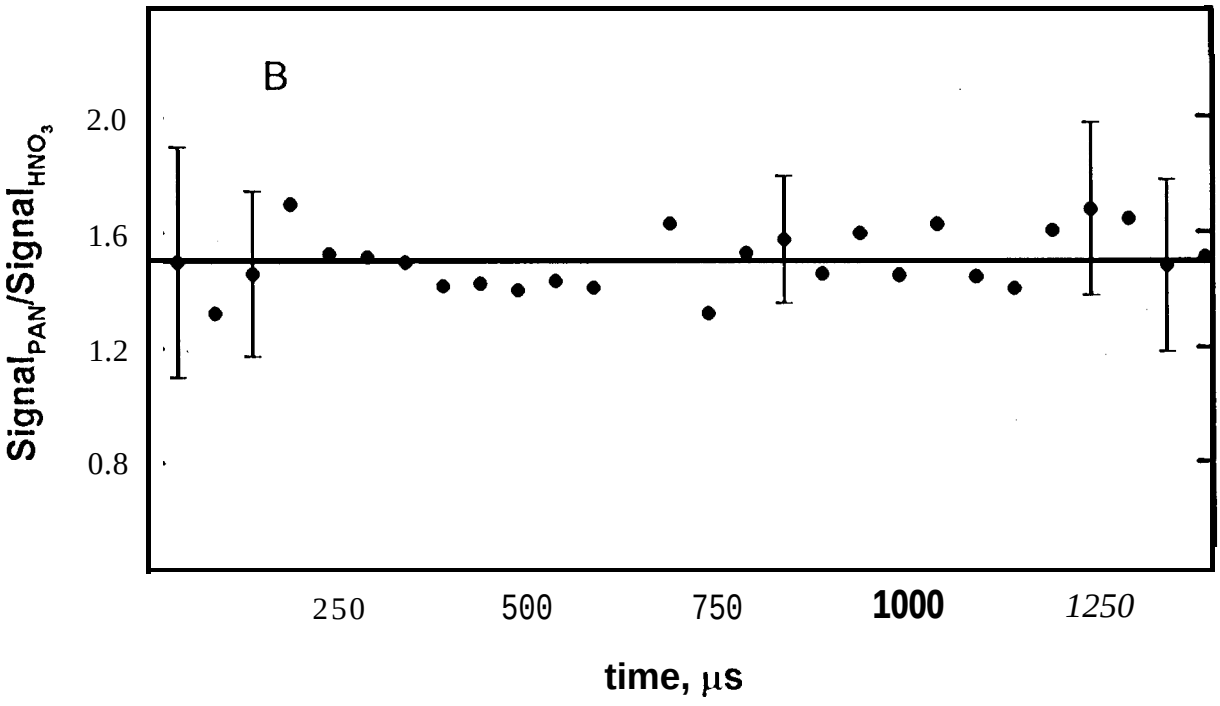
B
Signal$_{PAN}$/Signal$_{HNO_3}$
2.0
1.6
1.2
0.8
250
500
750
1000
1250
time, μs

Fig. 4

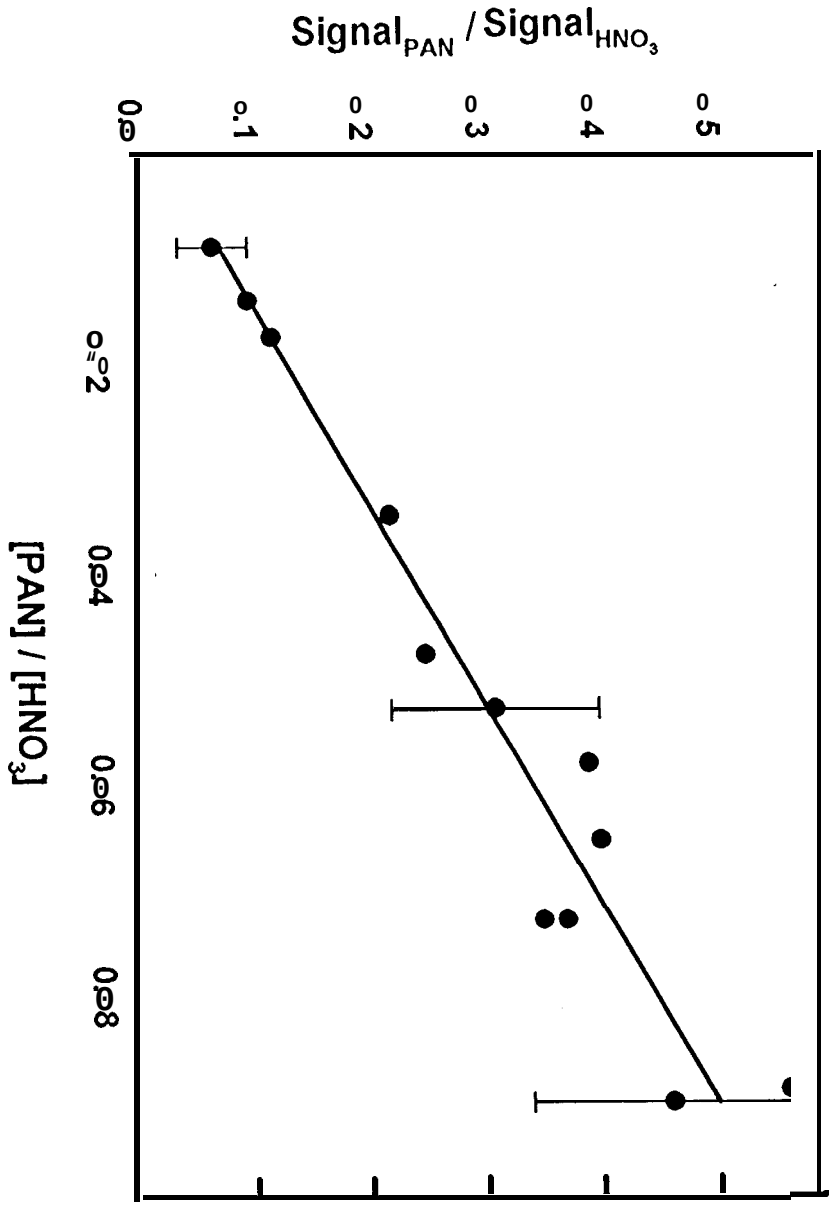
Signal$_{PAN}$ / Signal$_{HNO_3}$
0.0
0.1
0.2
0.3
0.4
0.5
0.02
0.04
0.06
0.08
[PAN] / [HNO$_3$]